10.1098/rspa.2002.0962

THE ROYAL SOCIETY

Long-wave forcing by the breaking of random gravity waves on a beach

By T. E. Baldock[1] and D. A. Huntley[2]

[1]*Department of Civil Engineering, University of Queensland, St Lucia, Queensland 4072, Australia*
[2]*Institute of Marine Studies, University of Plymouth, Drake Circus, Plymouth PL4 8AA, UK*

Received 3 July 2001; accepted 25 January 2002; published online 11 July 2002

This paper presents new laboratory data on long-wave (surf-beat) forcing by the random breaking of shorter gravity water waves on a plane beach. The data include incident and outgoing wave amplitudes, together with shoreline oscillation amplitudes at long-wave frequencies, from which the correlation between forced long waves and short-wave groups is examined. A detailed analysis of the cross-shore structure of the long-wave motion is presented, and the observations are critically compared with existing theories for two-dimensional surf-beat generation. The surf beat shows a strong dependency on normalized surf-zone width, consistent with long-wave forcing by a time-varying breakpoint, with little evidence of the release and reflection of incident bound long waves for the random-wave simulations considered. The seaward-propagating long waves show a positive correlation with incident short-wave groups and are linearly dependent on short-wave amplitude. The phase relationship between the incident bound long waves and radiated free long waves is also consistent with breakpoint forcing. In combination with previous work, the present data suggest that the breakpoint variability may be the dominant forcing mechanism during conditions with steep incident short waves.

Keywords: gravity water waves; breaking waves; long waves; surf beat; random waves; beaches

1. Introduction

Long-wave forcing by the breaking of shorter gravity water waves is an important mechanism for energy transfer in the coastal zone, where the higher-frequency wind or swell wave energy is transformed into a range of lower-frequency motions. These long-period waves were observed first outside the surf zone by Munk (1949) and Tucker (1950), and were termed surf beat due to a correlation with groups of high and low waves breaking further shoreward. Offshore of the surf zone, the lag between the incident short-wave groups and the surf beat corresponded with the time required for the groups to propagate to the shoreline and for a long wave to travel back to the measurement location. A large number of subsequent field studies have demonstrated the importance of surf-beat motions in the surf and swash zones, where surface elevation and velocity spectra are frequently dominated by low-frequency energy (Huntley *et al.* 1977; Guza & Thornton 1982, 1985; Wright *et al.* 1982). The long-period waves

may be propagating cross-shore (leaky waves), refractively trapped (edge waves) or a mixture of both modes (Suhayda 1974; Huntley *et al.* 1981; Oltman-Shay & Guza 1987) and are typically highly correlated with short-wave energy (Elgar *et al.* 1992; Herbers *et al.* 1995), consistent with generation by short waves. Surf beat is particularly significant in the nearshore zone, since long waves can modify the incident short-wavefield (Goda 1975; Peregrine 1983; Dally & Dean 1986) and strongly influence sediment transport patterns. In particular, long waves may enhance shoreline erosion (Osborne & Greenwood 1992) and, due to reflection, also lead to the formation of longshore bars, beach cusps and more complex morphology (Holman & Bowen 1982; O'Hare & Huntley 1994; Yu & Mei 2000).

Although a number of mechanisms for the generation of both leaky waves and edge waves have been proposed (Tucker 1950; Longuet-Higgins & Stewart 1962, 1964; Gallagher 1971; Symonds *et al.* 1982; Schäffer 1993), the mixture of wave modes on natural beaches, combined with directionally spread wavefields and varying topography, complicates the comparison of field data with theoretical models. In addition, previous laboratory work specifically focused on surf-beat-generation mechanisms has been limited to bichromatic wave groups (Kostense 1984; Baldock *et al.* 2000), where variations in the location of wave breaking predominantly occur at a single frequency, leading to a regular pattern of long-wave forcing. However, in real sea states, random wave breaking occurs over a broad range of space-time-scales and considerable uncertainty remains as to which surf-beat mechanisms are important or dominant during more realistic conditions (Battjes 1988; Hamm *et al.* 1993).

This paper considers this problem and focuses on two-dimensional long-wave forcing (cross-shore motions only) through carefully controlled laboratory experiments. Surf-beat generation by random wave breaking is compared quantitatively and qualitatively with two fundamentally different existing theories (Longuet-Higgins & Stewart 1962, 1964; Symonds *et al.* 1982), with agreements and discrepancies discussed in detail. The laboratory study includes measurements of incident and outgoing long waves, the correlation between forced long waves and random short-wave groups, the linear and nonlinear dependence of long-wave energy on short-wave amplitude, and a detailed analysis of the cross-shore structure of the long-wave motion. Section 2 commences with a brief review of previous work and a discussion of the expected characteristics of the forced long-wave motion. The experimental set-up and analysis techniques are outlined in § 3. Section 4 presents and discusses the experimental data, followed by final conclusions in § 5.

2. Previous work

Longuet-Higgins & Stewart (1962, 1964) showed that non-breaking short-wave groups nonlinearly force a long wave that is bound to the short-wave groups and negatively correlated with groups of large waves. They suggested that the release of this incident bound long wave during short-wave breaking, followed by subsequent reflection at the shoreline, could explain the observations of Tucker (1950), who found that seaward-propagating long waves appeared predominantly negatively correlated with shoreward-propagating groups of high waves. Janssen *et al.* (2000) found a similar negative correlation for short waves breaking directly onto a model breakwater, but this disappeared if breaking occurred further offshore. In contrast, Munk's (1949) data suggest a positive correlation between the surf beat and short-wave groups,

which is inconsistent with bound wave release as the primary surf-beat mechanism unless the released and reflected long wave undergoes a significant (near 180°) phase shift (Guza *et al.* 1984). Release and reflection of the incident bound long wave also implies that the amplitude of the seaward-propagating long waves should be approximately proportional to the square of the incident short-wave height (Battjes 1988), although the dependence may be weaker than quadratic, since larger waves break further offshore (Tucker 1950; Longuet-Higgins & Stewart 1962). However, the majority of field data typically show surf beat to be linearly dependent on short-wave amplitude (Guza & Thornton 1982; Elgar *et al.* 1992; Herbers *et al.* 1995; Ruessink 1998), whereas the incident bound wave amplitudes follow the expected quadratic dependence.

Symonds *et al.* (1982) subsequently proposed a model for surf-beat generation that was directly due to the variability of the short-wave breakpoint, and where the resulting long-wave amplitude is linearly proportional to the incident short-wave height. This model proposes that a time-varying breakpoint (due to varying incident short-wave heights) radiates long waves both seaward and shoreward. The shoreward-propagating long wave subsequently reflects at the shoreline, setting up an interference pattern that is dependent on the phase relationship between the two breakpoint-forced long waves. The amplitude of the final seaward-propagating wave then varies according to a non-dimensional measure of the surf-zone width, χ, given by

$$\chi = \frac{\omega^2 \bar{h}_{\mathrm{b}}}{g\beta^2}, \tag{2.1}$$

where ω is the long-wave frequency ($2\pi f$), $\bar{h}_{\mathrm{b}}$ is the water depth at the mean breakpoint position, g is the acceleration due to gravity and β is the beach slope. Symonds *et al.* (1982) show that maximum outgoing long-wave generation occurs for $\chi \approx 1.2$, with minimal long-wave forcing at $\chi \approx 3.7$. Qualitative support for the Symonds *et al.* (1982) breakpoint-forcing model was provided by the laboratory experiments of Kostense (1984), with Schäffer (1993) later finding better agreement with the data by extending the model to include continued short-wave forcing in the surf zone and the influence of the incident bound long wave outside the surf zone. More quantitative experimental support for the breakpoint-forcing model was recently presented by Baldock *et al.* (2000), again, however, for bichromatic wave groups only. O'Hare *et al.* (2000) also show that free long waves modulate the breakpoint of shorter regular waves, leading to further long-wave generation, which is consistent with the Symonds *et al.* (1982) model.

Numerical models capable of reproducing aspects of surf-beat generation are well advanced and have developed from the work of Hibberd & Peregrine (1979), Kobayashi *et al.* (1989), Van Leeuwen & Battjes (1990) and Madsen *et al.* (1997). Good qualitative agreement with field data was found by List (1992) and Herbers *et al.* (1995), with further models presented by Watson & Peregrine (1992), Roelvink (1993) and Van Dongeren *et al.* (1994), comparing well with laboratory data. More recently, the results from the Boussinesq model presented by Madsen *et al.* (1997) show very good agreement with the bichromatic wave group data from both Kostense (1984) and Baldock *et al.* (2000). However, a problem with many of the models is that it is frequently not possible to separate the different long-wave forcing mechanisms, although the separation is explicit in the model of List (1992). Nevertheless,

a more detailed analysis of future numerical modelling results would be beneficial in determining the fundamental long-wave-generation mechanisms.

Laboratory data, field data and numerical model results therefore, to some extent, support both the idea of bound wave release (Longuet-Higgins & Stewart 1962) and the breakpoint-forcing mechanism of Symonds *et al.* (1982). However, detailed laboratory experiments have been limited to studies of bichromatic wave groups and it is therefore difficult to quantify the importance of the two forcing mechanisms during more realistic random-wave conditions. Further experiments with random-wave forcing are consequently reported in this paper.

3. Experimental set-up

(*a*) *Wave flume and instrumentation*

The experiments were carried out in a wave flume 18 m long, 0.9 m wide, with a working water depth, h, of 0.8 m (figure 1). A plane beach (gradient $\beta = 0.1$) starts 5.65 m from the wave paddle. The origin of the horizontal coordinate, x, is taken as the intersection of the still-water line with the beach face, positive onshore. For unbroken monochromatic regular waves with frequencies of 0.1–0.4 Hz, the reflection coefficient for this beach ranges from 0.9 to 0.6, with negligible reflection (3–5%) for breaking waves in the frequency range 0.6–1 Hz. Waves were generated by a hydraulically driven wedge-type wave paddle using second-order generation for long waves (Barthel *et al.* 1983). A software-driven digital-feedback system absorbs up to 60% (in amplitude terms) of waves radiated from the far end of the flume for frequencies at 0.1 Hz, rising to over 90% above 0.4 Hz. The wave motion generated by the wave paddle is highly repeatable, allowing data to be collected at multiple cross-shore locations.

Data were collected simultaneously from an array of five surface-piercing resistance-type wave gauges, mounted on a carriage above the flume, and a run-up wire within the swash zone. The absolute accuracy of these wave gauges is of order ± 1 mm, with a relative accuracy better than ± 0.2 mm. The run-up wire consists of two 0.8 mm diameter stainless-steel wires 12 mm apart, held 3 mm above the bed, and has a resolution better than ± 0.5 mm in the vertical. Further details of both the wave flume and instrumentation may be found in Baldock *et al.* (2000).

(*b*) *Wave characteristics*

We examine data from eight random-wave simulations (Jonswap spectra (Hasselmann *et al.* 1973)) with varying peak frequency (f_p), target offshore root-mean-square wave height (H_rmso) and peak enhancement factor, γ. These cases are further subdivided into three series, depending on their peak frequency and spectral shape (table 1). Cases in series 1 have relatively narrow-banded frequency spectra ($f_\mathrm{p} = 0.6$ Hz, $\gamma = 3.3$, varying H_rmso), while those in series 2 are more broad banded ($f_\mathrm{p} = 0.6$ Hz, $\gamma = 1$, varying H_rmso). Series 3 has cases with both narrow- and broad-banded wave spectra ($f_\mathrm{p} = 1$ Hz, $H_\mathrm{rmso} = 0.05$ m, varying γ). These random simulations represent steep wave conditions ($H_\mathrm{rmso}/L_0 = 0.011$–$0.032$, where L_0 is the deep-water wavelength of the peak spectral frequency) compared with typical field data, with the occasional small spilling breaker occurring in the constant-depth region of the flume for some cases. The lower- and upper-frequency limits for the

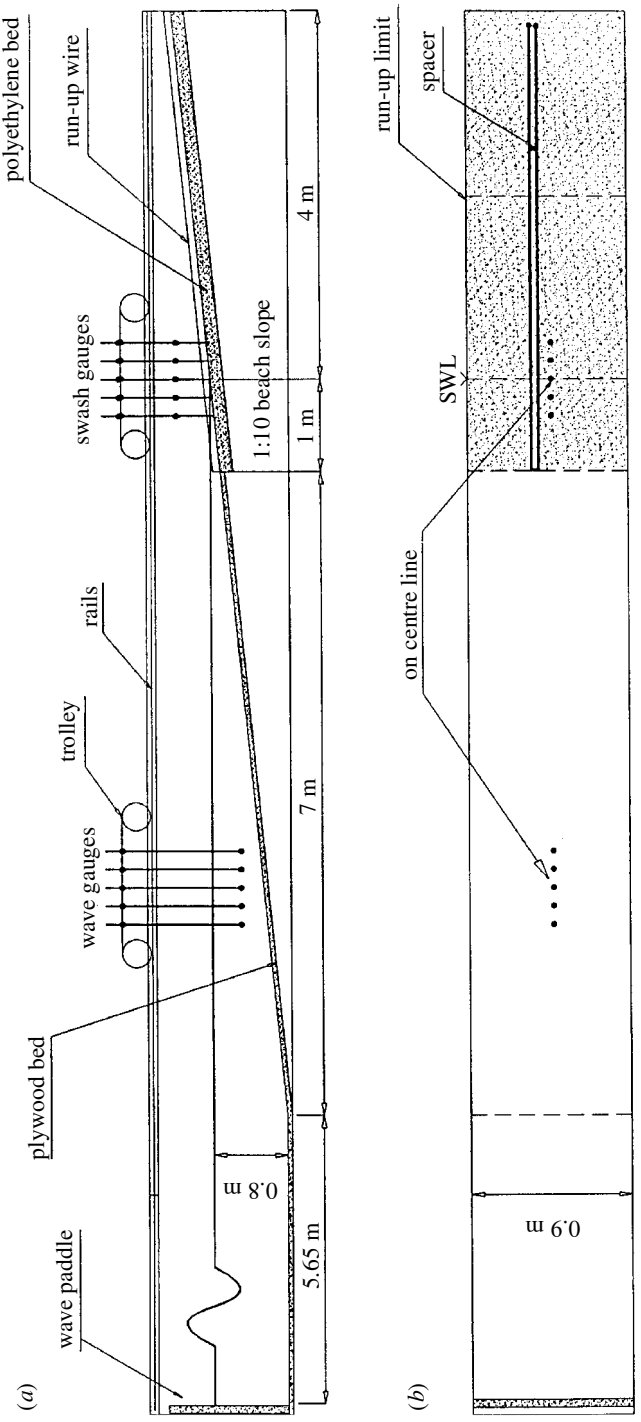

Figure 1. Wave flume and instrumentation.

Table 1. *Spectral characteristics, Iribarren number and mean breakpoint depth*

series	case	f_p (Hz)	f_1 (Hz)	f_2 (Hz)	γ	H_{rmso} (m)	ξ	h_b (m)
1	J6033A	0.6	0.42	1.47	3.3	0.1	0.61	0.07
	J6033B	0.6	0.42	1.47	3.3	0.075	0.71	0.053
	J6033C	0.6	0.42	1.47	3.3	0.05	0.87	0.035
2	J6010A	0.6	0.41	1.48	1.0	0.1	0.61	0.07
	J6010B	0.6	0.41	1.48	1.0	0.075	0.71	0.053
	J6010C	0.6	0.41	1.48	1.0	0.05	0.87	0.035
3	J1033C	1.0	0.67	1.78	3.3	0.05	0.56	0.035
	J6010C	1.0	0.65	1.74	1.0	0.05	0.56	0.035

primary (linear) wave components of the energy spectra, f_1 and f_2, respectively, are also given in table 1, from which long-wave frequencies are defined for the purpose of the present study as $f < 0.4$ Hz. The surf similarity parameter, or Iribarren number ($\xi = \beta/\sqrt{H_{rmso}/L_0}$) is in the range 0.56–0.87, indicating largely plunging breakers. The depth at the mean position of the breakpoint, $\bar{h}_b$, was taken at the location where approximately half the offshore incident wave energy would be dissipated, i.e. $(H_{rms}/H_{rmso})^2 = 0.5$. This may be written as

$$\bar{h}_b = \frac{1}{\kappa}\frac{\sqrt{2}}{2}H_{rmso}, \tag{3.1}$$

where κ is the ratio of the wave height to water depth at breaking. From a series of monochromatic wave measurements, κ has been taken equal to 1, typical of steep beaches, and the resulting values for $\bar{h}_b$ are shown in table 1.

For series 1 and 2, although the phases of individual frequency components within the frequency spectra were randomly distributed between zero and 2π, the same phases were used for the three cases in each series, i.e. cases J6033A–C and cases J6010A–C. Consequently, at the wavemaker, the three individually generated random-wave trains in each of series 1 and series 2 are identical apart from a change in amplitude. Their group structure, therefore, is effectively the same and, as a result, a very similar pattern of wave breaking should occur for each of the three cases in these two series. Consequently, any differences in long-wave generation due to variations in short-wave phase should largely be eliminated when considering the effects of short-wave nonlinearity (varying H_{rmso}, see §§ 4 *b* and 4 *d*).

(*c*) *Analysis techniques*

Spectral estimates ($S(f)$) were obtained from Fourier transforms of eight 50% overlapping data segments, each comprising 2048 data points sampled at 25 Hz, with frequency smoothing over three adjacent frequencies (0.036 Hz). The amplitude, $a(f_c)$, of the long-wave motion within finite frequency bands centred on f_c was estimated using the relationship

$$a(f_c) = \sqrt{2\int_{f_c-\delta f}^{f_c+\delta f} S(f)\,\mathrm{d}f}, \tag{3.2}$$

where $\delta f = 0.018$ Hz and is half the width of the finite frequency band and $S(f)$ is the spectral density of the water surface elevation. Wave heights were estimated from the variance, m_0, of measured surface elevation time-series ($H_{\mathrm{rms}} = \sqrt{8m_0}$), assuming a narrow-banded Gaussian process and a Rayleigh wave-height probability density function). Note that each random-wave case may be considered to be deterministic, rather than a single realization of random data, and therefore the spectra shown later do not require the confidence limits associated with stochastic processes (Baldock *et al.* 1996).

Previous studies (e.g. Guza *et al.* 1984; Elgar & Guza 1985; List 1992; Masselink 1995) have used linear theory to crudely separate time-series of incident and outgoing long waves in natural random sea states. However, such an analysis ignores the nonlinearity of the incident bound long waves and the influence of the bed slope, and may therefore be subject to considerable errors, particularly close to the breakpoint. The present paper therefore attempts to adopt a more rigorous approach and, in particular, does not attempt to separate incident and outgoing waves on the sloping bed close to the breakpoint where the bound wave attains maximum amplitude. Indeed, this is not necessary since the incident and outgoing long waves are generally well separated in time (see § 4 *c* below). Decomposition of the total long-wave energy into free and bound long waves by bispectral analysis (e.g. Hasselmann *et al.* 1963; Herbers *et al.* 1994, 1995; Ruessink 1998) is not well suited to the present data due to the relatively short record lengths (420 s) and the nature of the time-series, which are not true stochastic processes. However, again this is unnecessary, since the experiments were designed to quantify long-wave nonlinearity directly (cf. § 4 *d*).

Although it is simple to separate incident bound long waves, incident free waves and reflected free waves for a bichromatic short-wave group (Kostense 1984), this is not the case in a random sea state, where different pairs of short waves may generate bound long waves at the same frequency but with different wavenumbers, and vice versa. Therefore, in order to estimate the amplitudes of incident and outgoing free long waves in the constant-depth region of the flume ($x < -8$ m), it was first necessary to calculate the contribution to the measured water surface elevation from incident bound long waves. These calculations were based on the original finite-depth solution for pairs of interacting small-amplitude wave components due to Longuet-Higgins & Stewart (1960). This solution was previously shown to give good agreement with measured data from bichromatic wave groups in the same experimental facility (Baldock *et al.* 2000). In addition, Lo & Dean (1995) show that the Longuet-Higgins & Stewart (1960) solution is accurate provided $h/L_0 > 0.1$, a condition satisfied for all wave cases for $x < -4$ m. The calculations were carried out over the range f_2–f_1, i.e. only considering the primary components of the measured wave spectra. However, some small errors may be introduced by second- and higher-order interactions, which modify the original (linear) spectral density within the primary frequency band f_2–f_1 (Freilich & Guza 1984; Baldock *et al.* 1996).

The calculated second-order bound long waves were subsequently subtracted from Fourier-filtered low-pass ($f < 0.4$ Hz) measured surface-elevation data, theoretically resulting in a surface-elevation time-series comprised solely of incident and outgoing free long waves. The incident and outgoing free long-wave surface-elevation time-series were then separated using the two-gauge method of Frigaard & Brorsen (1995), from which both incident and outgoing long-wave spectra and amplitudes could be readily determined.

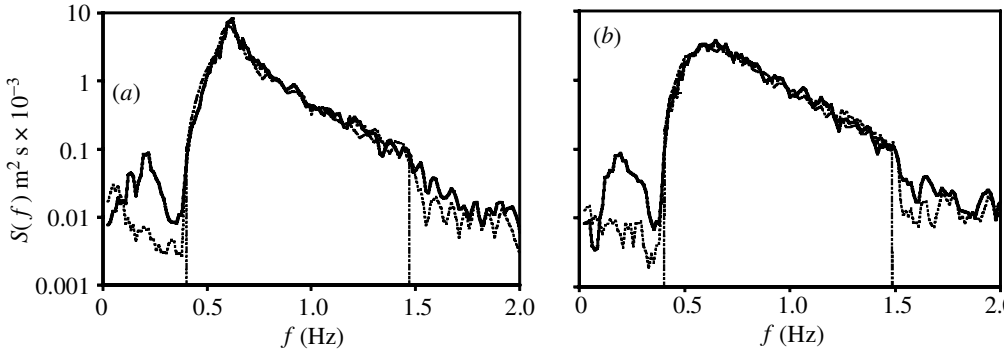

Figure 2. (*a*) Total wave energy spectra, case J6033A, $H_{\mathrm{rms0}} = 0.1$ m. (*b*) Total wave energy spectra, case J6010A, $H_{\mathrm{rms0}} = 0.1$ m. (Solid line, measured ($x = -11.15$ m); dot-dashed line, first order; dashed line, second order.)

The normalized cross-correlation signal, $R_{xy}(\tau)$, between two time-series $x(t)$ and $y(t)$ was estimated by (Bendat & Piersol 1986)

$$R_{xy}(\tau) = \frac{\langle x(t)y(t+\tau)\rangle}{\sigma_x \sigma_y}, \tag{3.3}$$

where τ is the time lag between the two signals, σ_x and σ_y are the standard deviations of the respective time-series, $\langle\cdot\rangle$ denotes ensemble averaging and $-1 \leqslant R_{xy}(\tau) \leqslant 1$. In this instance, the two time-series are the low-pass filtered ($f < 0.4$ Hz) long-wave surface elevation and the envelope of the short-wave surface elevation, $A(t)$, at various cross-shore locations. The short-wave envelope is readily obtained via a Hilbert transform of the measured surface-elevation data (Sobey & Liang 1986). The normalized cross-correlations were calculated using 4096 data points sampled at 25 Hz, giving, for the present data, a 95% confidence interval on $R_{xy}(\tau) = 0$ of approximately ± 0.18 (Jenkins & Watts 1968; Garrett & Toulany 1981).

Note that the cross-correlation analysis shows the lag, or time-domain separation, between the short-wave groups and any associated long-wave motion. Consequently, at measurement locations seaward of the breakpoint, incident and outgoing long waves are well separated in the correlation signal. It is therefore not necessary to separate the incident and reflected waves prior to the correlation analysis. Possible errors introduced by applying linear theory to shoaling nonlinear waves were therefore avoided by using the total long-wave surface-elevation time-series.

4. Discussion of results

(*a*) *Spectral characteristics and cross-shore variation in wave height*

Figure 2 shows examples of the surface-elevation energy spectra in the constant-depth region of the wave flume ($x < -8$ m) for case J6033A (narrow banded) and case J6010A (broad banded). The measured data are in good agreement with both the target first-order spectra in the primary frequency band (f_2–f_1) and the higher harmonics ($f > f_2$) in the calculated second-order spectra, which arise through wave–wave interactions between the primary components (Longuet-Higgins & Stewart 1960). However, the measured data show considerable deviations from the second-

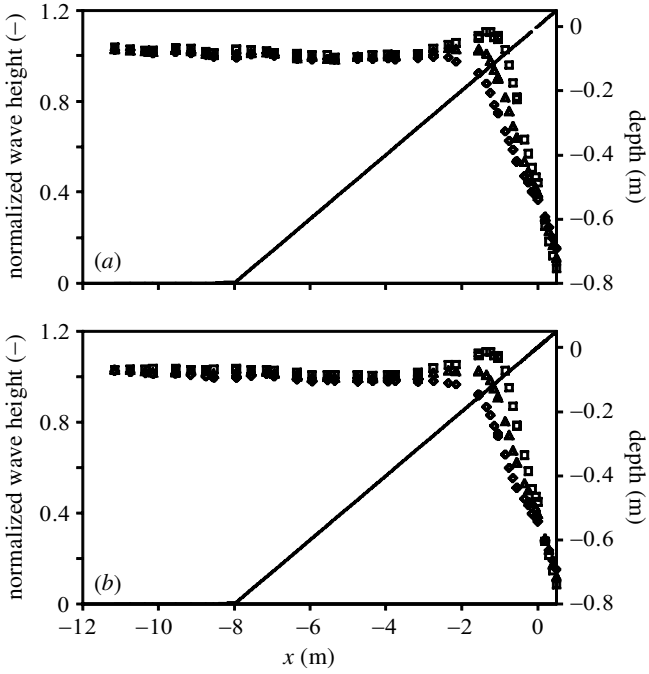

Figure 3. (*a*) Cross-shore variation in normalized H_{rms} wave height, series 1, $\gamma = 3.3$. (◊, case J6033A; △, case J6033B; □, case J6033C.) (*b*) Cross-shore variation in normalized H_{rms} wave height, series 2, $\gamma = 1$. (◊, case J6010A; △, case J6010B; ▫, case J6010C.)

order spectra in the long-wave frequency band ($f < 0.4$ Hz), suggesting that significant additional free long-wave energy is present in the wave flume at this location. This additional energy is predominantly contained in the frequency band 0.1–0.3 Hz. The second-order spectra additionally show that the bound long-wave energy is greatest in the frequency band $0.05 < f < 0.1$ Hz.

The cross-shore variation in wave height (H_{rms}) for the three cases in each of series 1 and series 2 is shown in parts (*a*) and (*b*) of figure 3, respectively. The measured data have been normalized by the target H_{rmso} for each case (table 1) and are typically within 3% of this value close to the wavemaker. Figure 3 shows that the outer breakpoint, or the furthest offshore location of depth-induced wave breaking, is around $x = -2$ m for $H_{\mathrm{rmso}} = 0.1$ m, moving further shoreward to about $x = -1$ m for $H_{\mathrm{rmso}} = 0.05$ m. The position of the mean breakpoint (normalized wave height equal to $\frac{1}{2}\sqrt{2}$) is additionally in good agreement with the estimates based on (3.1).

(*b*) *Incident and radiated long-wave amplitudes*

Although some reflection is possible from the sloping beach seaward of the surf zone, and wave groups propagating up a slope may generate both incident and outgoing free long waves (Mei & Benmoussa 1984; Bird & Peregrine 1998), in the following we assume that all outgoing free long waves are generated shoreward of the outer breakpoint by one or more of the mechanisms discussed in § 2. This largely appears to be confirmed by the cross-shore nodal structure of the long-wave motion (see § 4 *e*).

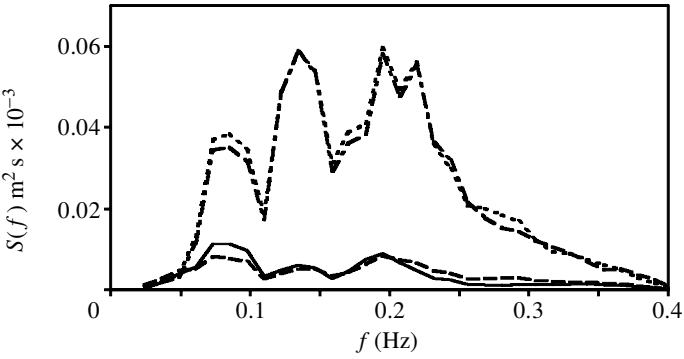

Figure 4. Incident and reflected free long-wave energy spectra, case J6033A, $H_{\mathrm{rms0}} = 0.1$ m. (Solid line, incident ($x = -11.15$ m); dot-dashed line, reflected ($x = -11.15$ m); long-dashed line, incident ($x = -9.55$ m); short-dashed line, reflected ($x = -9.55$ m).)

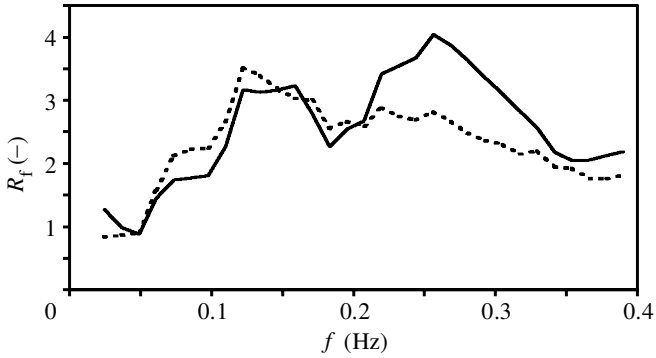

Figure 5. Variation in free long-wave radiation coefficient with frequency, case J6033A, $H_{\mathrm{rms0}} = 0.1$ m. (Solid line, $x = -11.1$ 5m; dashed line, $x = -9.55$ m.)

Figure 4 shows incident and outgoing free long-wave energy spectra for case J6033A, estimated at two different locations in the constant-depth region of the flume ($x < -8$ m) by the method outlined in § 3 *c*. The outgoing long-wave energy spectra show the clear frequency response expected according to the Symonds *et al.* (1982) breakpoint-forcing model, with the peak response at *ca.* 0.2 Hz. This peak frequency corresponds to a value of $f/\beta \approx 2$, very similar to the value for bichromatic wave groups found by Madsen *et al.* (1997) and Baldock *et al.* (2000). The data from both locations give very consistent results and suggest that the additional long-wave energy at $f < 0.4$ Hz observed in figure 2 is predominantly outgoing and radiated from shoreward of these measurement locations.

This is further illustrated in figure 5, which shows the ratio of the outgoing to incident free long-wave amplitude (R_{f}), where the long-wave amplitude was obtained from the energy spectra shown in figure 4, again as outlined in § 3 *c*. R_{f} is a radiation coefficient, rather than a reflection coefficient, since most of the outgoing free wave energy is generated shorewards of the measurement points ($x < -8$ m). In addition, according to the breakpoint-forcing theory, approximately half of this wave energy may be radiated directly offshore and never reflects at the shoreline. The radiation coefficient is typically greater than 2 over the frequency range $0.1 < f < 0.4$, consistent with minimal free long-wave generation and good long-wave absorption

at the wavemaker. Note that, in theory, infinite radiation coefficients should occur, since both Symonds *et al.* (1982) and Schäffer (1993) assume incident free long-wave energy is zero. In contrast, field measurements are complicated by refractive trapping of long waves and, as a result, typically show reflection/radiation coefficients much closer to one (Herbers *et al.* 1995).

In order to compare the measured data directly with the breakpoint-forcing model of Symonds *et al.* (1982), the amplitudes of the outgoing free long waves at the outer breakpoint are required. These were estimated from the measurements in the constant-depth region of the flume ($x < -8$ m) using full linear shoaling. In Symonds *et al.* (1982), these amplitudes were subsequently normalized by half the difference in shoreline set-up, $\frac{1}{2}\bar{\eta}$, produced by monochromatic waves with heights corresponding to the largest and smallest short waves within the wave group, which may be easily estimated for bichromatic wave groups (Baldock *et al.* 2000). However, in a random sea state, both the period and amplitude of the wave groups vary and, therefore, the amplitudes of the largest and smallest waves within individual groups are frequency dependent. Consequently, an equivalent measure of the shoreline set-up was determined from the spectrum of the offshore short-wave surface-elevation envelope, $A(t)$. This provides an estimate of how the amplitude modulation, or groupiness, of the surface elevation varies with frequency. List (1991) shows that this technique may be used to provide an estimate of the overall surface-elevation groupiness, G, given by

$$G = \frac{\sqrt{2\sigma_{A(t)}}}{\overline{A(t)}}, \tag{4.1}$$

where $\sigma_{A(t)}$ is the standard deviation of the short-wave envelope. Based on measurements in the constant-depth region of the flume, equation (4.1) gives groupiness values for the random-wave cases considered here in the range 0.7–0.8, typical of natural sea states (List 1991).

For a bichromatic wave group, the numerator of (4.1) is equivalent to ΔA, the difference in amplitude between the largest and smallest waves in the group, the denominator is the mean wave height, and $G = 1$ for a fully modulated wave group. Hence, for a random sea state and following (3.2), the variation in wave group amplitude with frequency, $a_G(f)$, may be written as

$$a_G(f_c) = \sqrt{2\int_{f_c-\delta f}^{f_c+\delta f} S_A(f)\,\mathrm{d}f}, \tag{4.2}$$

where $S_A(f)$ is the spectral density of the short-wave surface-elevation envelope. Since $A(t)$ is poorly defined both at the outer breakpoint and within the surf zone due to increased nonlinearity and broadbandedness in shallow water (Sobey & Liang 1986; Huang *et al.* 1999), equation (4.2) uses $A(t)$ calculated in the constant-depth region of the wave flume ($x < -8$ m). This assumes that changes in the overall time-averaged wave-group characteristics are relatively minor between deep and shallow water, i.e. the shoaling characteristics of both large and small waves are similar. Although nonlinear shoaling leads to significant changes in the shape of individual waves (e.g. Elgar & Guza 1985), this assumption nevertheless appears consistent with data from List (1991), Watson *et al.* (1994) and Bird & Peregrine (1998), which show that both groupiness and wave-group structure are fairly consistent prior to wave breaking.

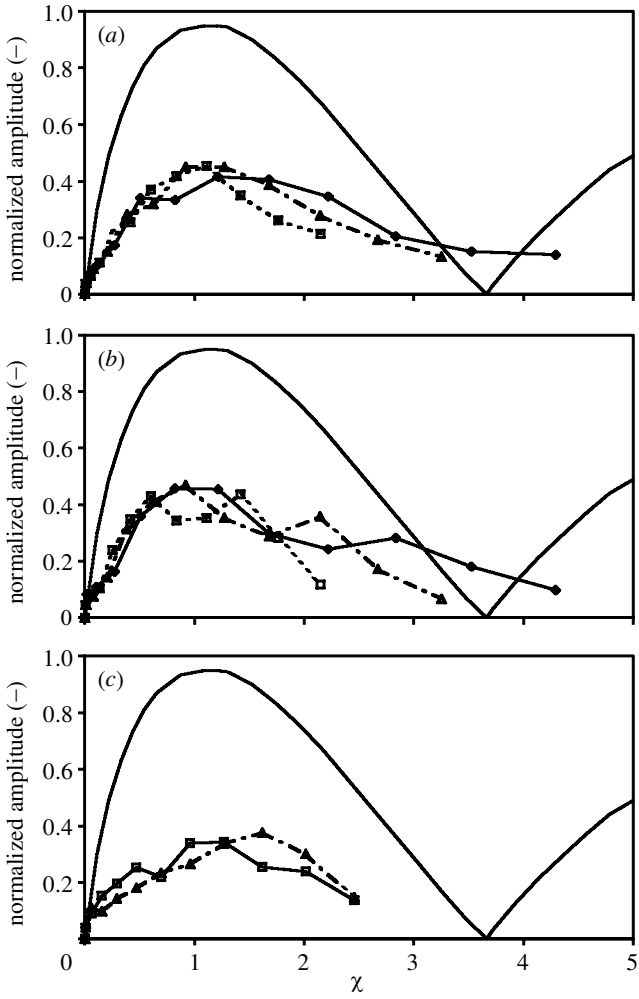

Figure 6. (*a*) Normalized outgoing free wave amplitude versus χ, series 1, $\gamma = 3.3$. (◊, case J6033A; △, case J6033B; ▫, case J6033C; solid line, Symonds *et al*. (1982), $G = 0.2$.) (*b*) Normalized outgoing free wave amplitude versus χ, series 2, $\gamma = 1$. (◊, case J6010A; △, case J6010B; ▫, case J6010C; solid line, Symonds *et al*. (1982), $G = 0.2$.) (*c*) Normalized outgoing free wave amplitude versus χ, series 3. (▫, case J1033C; △, case J1010C; solid line, Symonds *et al*. (1982), $G = 0.2$.)

Following Longuet-Higgins & Stewart (1964), $\frac{1}{2}\bar{\eta}$ at discrete frequencies, f_c, was then estimated by

$$\tfrac{1}{2}\bar{\eta}(f_c) = \tfrac{1}{2}(\tfrac{3}{2}(\tfrac{1}{2}\kappa)(2a_G(f_c))). \tag{4.3}$$

The outgoing long-wave amplitudes at the outer breakpoint were subsequently normalized by (4.3), with the corresponding values of χ calculated from (2.1) using the tabulated values of $\bar{h}_b$ given previously. The results are compared with the theoretical response for breakpoint-forced long waves given by Symonds *et al*. (1982) in figure 6. All three series show a maximum response in the range $\chi \approx 1$–1.4, close to that expected from theory and similar to that found previously for bichromatic

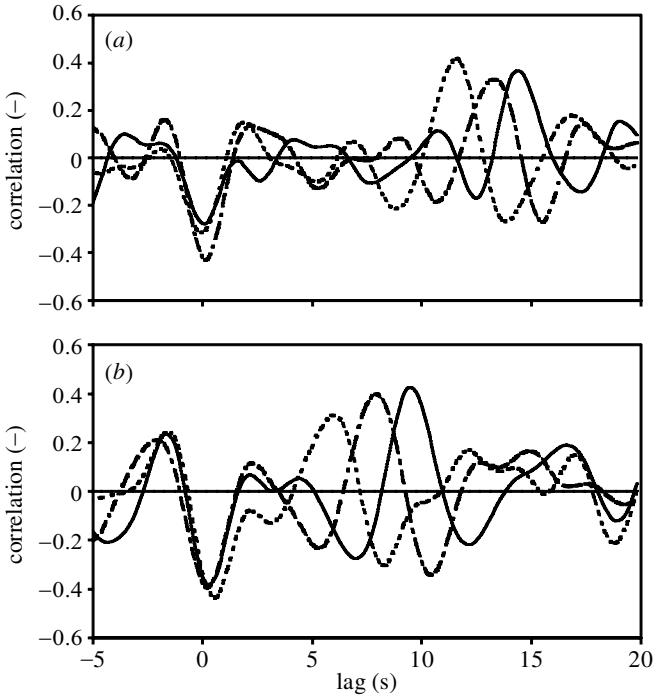

Figure 7. Cross-correlation between the local wave envelope and the local low-frequency motion seaward of the breakpoint, case J6010A. (*a*) Solid line, $x = -11.15$ m; dot-dashed line, $x = -9.55$ m; dashed line, $x = -7.95$ m. (*b*) Solid line, $x = -6.35$ m; dot-dashed line, $x = -4.75$ m; dashed line, $x = -3.15$ m.

wave groups by Baldock *et al.* (2000). In addition, the response curve for the individual cases within each series is very similar, indicating that the long-wave generation process is linearly dependent on the amplitude of the incident short waves. The data also show that the normalized response is insensitive to differences in spectral shape, consistent with the relatively constant wave groupiness noted above. Note that, although the maxima are significantly smaller than the theoretical value for a groupiness factor, G, equal to 0.2, this is consistent with Symonds *et al.* (1982), who show that the normalized response reduces rapidly as the wave-group modulation increases. Unfortunately, the assumption of a small breakpoint excursion by Symonds *et al.* (1982) and Schäffer (1993) restricts the theoretical analysis to small values of G, and no analytical solution is presently available for $G > 0.5$.

(*c*) *Relationship between the short-wave envelope and the low-frequency motion*

The normalized cross-correlations between the local short-wave envelope and the local low-frequency motion ($f < 0.4$ Hz) at various locations seaward of the breakpoint are shown in figure 7 for case J6010A. Very similar cross-correlation signals are obtained for the other random-wave cases (not shown), although the correlations are weaker for the smallest wave heights ($H_{\mathrm{rmso}} = 0.05$ m). A relatively strong negative correlation occurs at a lag $\tau = 0$, corresponding to the locally forced bound long wave, which is out of phase with the local short-wave envelope (Longuet-Higgins

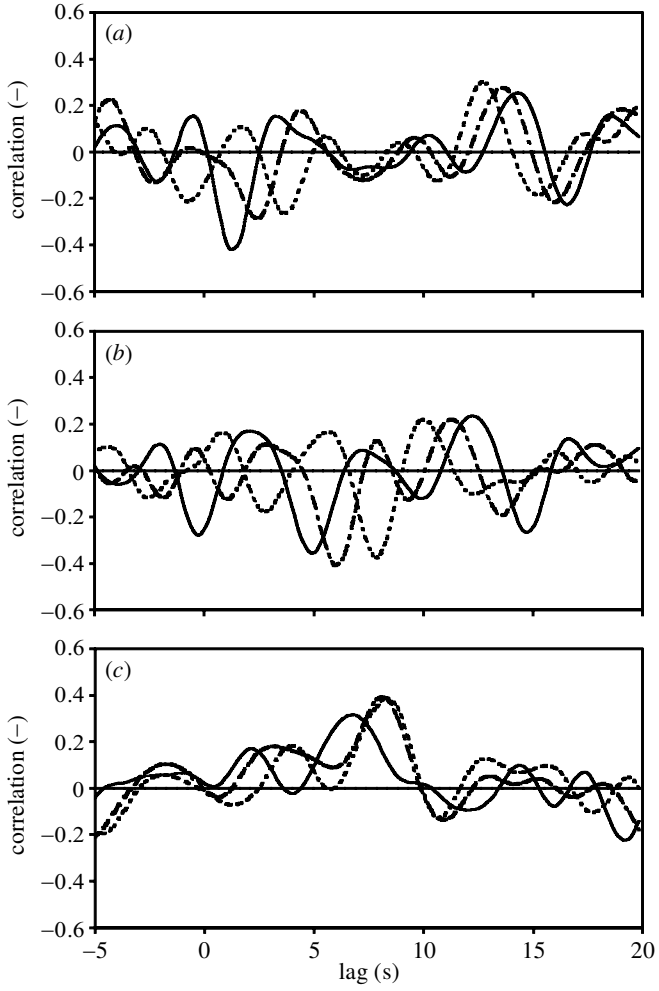

Figure 8. Cross-correlation between the wave envelope at $x = -11.15$ and the low-frequency motion at more shoreward locations, case J6010A. (*a*) Solid line, $x = -9.55$ m; dot-dashed line, $x = -7.95$ m; dashed line, $x = -6.35$ m. (*b*) Solid line, $x = -4.75$ m; dot-dashed line, $x = -3.15$ m; dashed line, $x = -1.55$ m. (*c*) Solid line, $x = -0.55$ m, dot-dashed line, $x = -0.05$ m; dashed line, run-up.

& Stewart 1962, 1964). Close to the outer breakpoint ($x = -3.15$ m), the bound long wave appears to lag slightly behind the short-wave envelope, although this appears less marked than that observed in field and laboratory data obtained from more mildly sloping beaches (Elgar & Guza 1985; List 1992; Janssen *et al.* 2000). A strong positive correlation is observed at $\tau \approx 15$ s at the furthest offshore location ($x = -11.15$ m), with the lag progressively reducing to $\tau \approx 6$ s just seaward of the outer breakpoint. This peak in the correlation signal corresponds to a long wave positively correlated with the local wave envelope, and the data strongly suggest that this long wave is travelling offshore.

This is further illustrated in figure 8, which shows the cross-correlation between the short-wave envelope at $x = -11.15$ m and the low-frequency motion further

shoreward. Seaward of the breakpoint, both the negative and positive peaks in the correlation signal remain separated in time and lead to similar conclusions to those reached above. However, inside the surf zone, and in the run-up, the correlation signal evolves to show a single dominant long wave, positively correlated with the offshore wave envelope. This is to be expected, since larger incident waves will produce a larger dynamic set-up, and follows directly from the breakpoint-forcing model of Symonds *et al.* (1982). Some additional low-frequency motion, both at the shoreline and in the surf zone, will also be generated due to continued wave groupiness and mass transport by short waves, which again will be positively correlated with the incident wave groups (Watson & Peregrine 1992).

For the data presented in figures 7 and 8, the time lag observed at each cross-shore location approximately corresponds to the time taken for a wave group to travel to the breakpoint, plus the time required for a long wave to travel from the breakpoint to the shore and then back to the measurement position, as first suggested by Munk (1949) and Tucker (1950). Similar time lags also have been observed in subsequent field data, typically from mildly sloping beaches (Guza *et al.* 1984; List 1992; Masselink 1995), although the correlations between the long wave and wave envelope suggest an outgoing positive pulse leading a slightly larger long wave trough. This positive–negative correlation has usually been interpreted as due to an incident bound long wave developing an asymmetric form during shoaling, which is then subsequently released at the breakpoint and reflected from the shoreline (List 1992; Masselink 1995).

In contrast, the present data show that the outgoing long wave is predominantly positively correlated with the incident wave groups, in agreement with the breakpoint-forcing model. Furthermore, the positive correlation in the inner surf zone and in the run-up (figure 8*c*) is inconsistent with the release of the negatively correlated bound long wave observed just prior to breaking (figure 7). The present data also show a weak long-wave trough lagging the dominant outgoing positive surface elevation. This is probably generated by the run-down of the water mass forced up the beach face by incident short-wave bores reaching the shoreline with some remaining group structure (Watson & Peregrine 1992).

(*d*) *Linear and nonlinear long-wave dependence on short-wave amplitude*

Figure 9 shows the cross-shore variation in the total (incident and outgoing) long-wave energy within finite frequency bands centred on f_c (i.e. $f_c \pm 0.018$ Hz). The data are shown for series 1 and have been normalized by the square of the target incident wave height (H^2_{rmso}), or short-wave energy, for each case (table 1). Offshore of the breakpoint ($x < -2$ m), the energy at low frequencies ($f_c = 0.097$–0.134 Hz; figure 9*a*,*b*) is nonlinearly dependent on the offshore short-wave energy, and in fact the long-wave amplitude is almost exactly proportional to the square of the short-wave amplitude. The long-wave motion offshore of the breakpoint at these frequencies is therefore dominated by incident bound long waves, consistent with the observed weak free outgoing long wave (figure 4).

Conversely, at these same frequencies ($f_c = 0.097$–0.134 Hz; figure 9*a*,*b*) inside the breakpoint ($x > -2$ m) and in the run-up (most shoreward data points and plotted at the mean shoreline position), the long-wave energy appears much more linearly dependent on the offshore short-wave energy. Indeed, the change from relatively

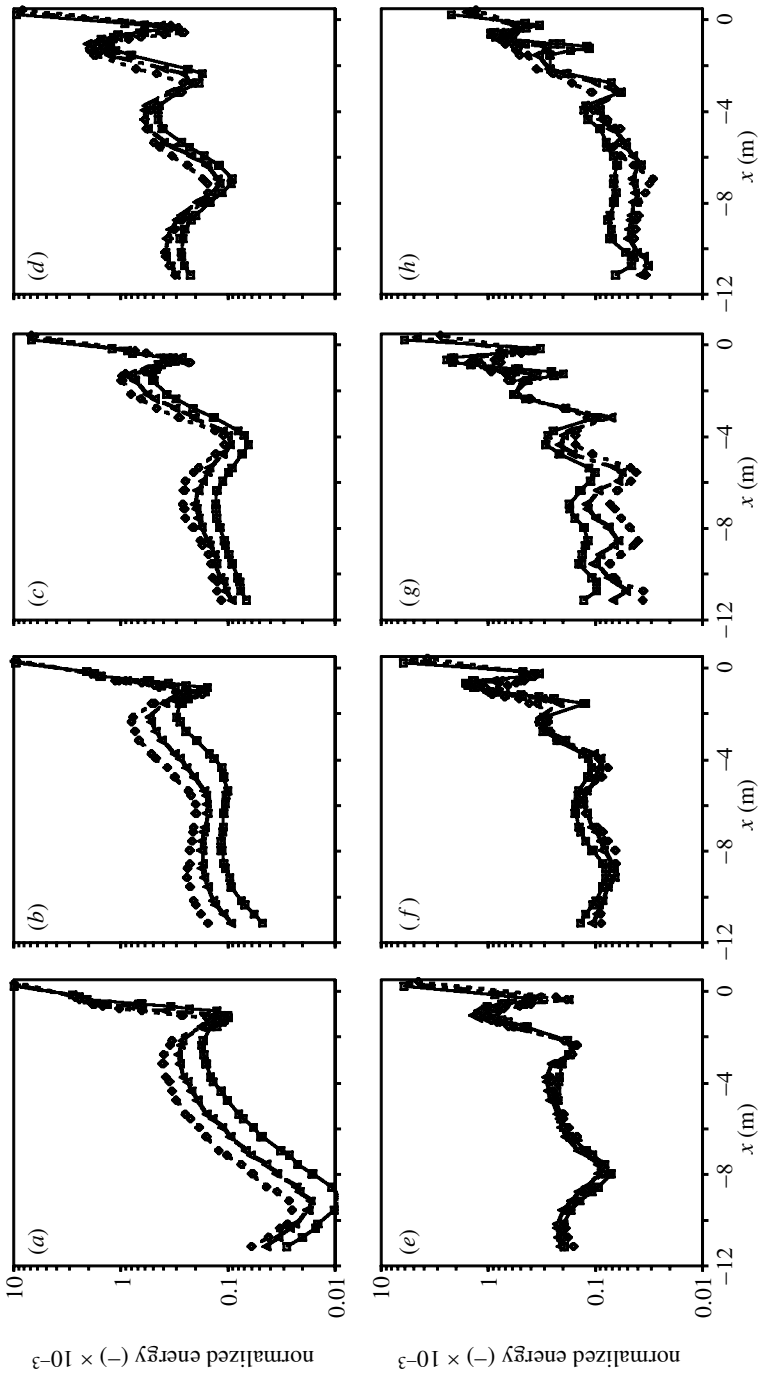

Figure 9. The cross-shore variation in the normalized wave energy within frequency band $f_c \pm 0.018$ Hz, series 1, $\gamma = 3.3$. (*a*) $f_c = 0.097$ Hz; (*b*) $f_c = 0.134$ Hz; (*c*) $f_c = 0.17$ Hz; (*d*) $f_c = 0.207$ Hz; (*e*) $f_c = 0.244$ Hz; (*f*) $f_c = 0.218$ Hz; (*g*) $f_c = 0.317$ Hz; (*h*) $f_c = 0.354$ Hz. (◇, case J6033A; △, case J6033B; ▫ , case J6033C.)

strong nonlinear motion just offshore of the breakpoint to nearly linear motion in the inner surf zone suggests that the incident bound wave energy is strongly dissipated by the breaking process, with subsequent long-wave generation by the time-varying breakpoint forcing. This is considered further in § 4 *e*, where more detailed data from the individual random-wave cases is presented.

At higher frequencies ($f_c = 0.17$–0.244 Hz; figure 9*c*–*e*), the total long-wave motion becomes progressively more linear both offshore and shoreward of the breakpoint, and at $f_c = 0.244$ Hz (figure 9*e*), the long-wave energy is almost exactly linearly proportional to the offshore short-wave energy at all cross-shore locations. The long-wave amplitude is therefore also linearly dependent on the short-wave amplitude and this frequency ($f_c = 0.244$ Hz) corresponds well with the peak spectral frequency of the outgoing free long waves (figure 4). The total long-wave motion at this frequency appears, therefore, to be dominated by free long waves, consistent with the surface-elevation spectra shown in figure 2. The cross-shore nodal structure is strongest in the frequency range $f_c = 0.17$–0.207 Hz, where a combination of incident bound waves and outgoing free waves occurs. At both lower and higher frequencies, the nodal structure is weaker, due to dominance of the total long-wave motion by either incident bound waves or outgoing free waves, respectively. The reason for this is that the overall long-wave motion tends to be dominated by waves propagating in one direction only, thereby leading to a less-marked nodal structure. This cross-shore nodal structure is discussed further, again in § 4 *e*.

These data are in general agreement with field data showing a roughly linear relationship between offshore wave height and free long-wave amplitude (Guza & Thornton 1982; Elgar *et al.* 1992; Herbers *et al.* 1995). However, previous analyses of field data have not examined how the relationship between the total long-wave energy (or bound/free long-wave energy) and the offshore wave energy varies with long-wave frequency. In particular, if bound and free long-wave energy dominate the total long-wave motion at different frequencies, as is the case here, then this would appear inconsistent with the hypothesis of bound wave release as the primary mechanism for the generation of free long waves.

At still higher frequencies ($f_c = 0.281$–0.354 Hz; figure 9*f*–*h*), the data show that the relationship between the long-wave motion and offshore short-wave height is weaker than linear, particularly seaward of the breakpoint. Given that free outgoing long waves also dominate the total long-wave motion at these frequencies (figures 2 and 4), this implies that the long-wave generation, either at the breakpoint or within the surf zone, is weaker than linearly proportional to the offshore wave height. A possible reason for this is that the breakpoint-forcing mechanism will become ineffective when the breakpoint excursion, and hence the forcing region, becomes large in comparison with the wavelength of the long-wave motion. Baldock *et al.* (2000) suggested that this will occur when

$$\frac{G\sqrt{H}f_{\mathrm{L}}}{\beta\sqrt{g}} > \alpha, \tag{4.4}$$

where f_{L} is the long-wave frequency and α is some fraction of the wavelength of the free long wave, estimated to lie in the range 0.2–0.3. Applying (4.4) to the present conditions, with $H = H_{\mathrm{rms}} = 0.1$ m, suggests that the breakpoint forcing will start to become ineffective for the larger wave heights when f_c is greater than *ca.* 0.3 Hz,

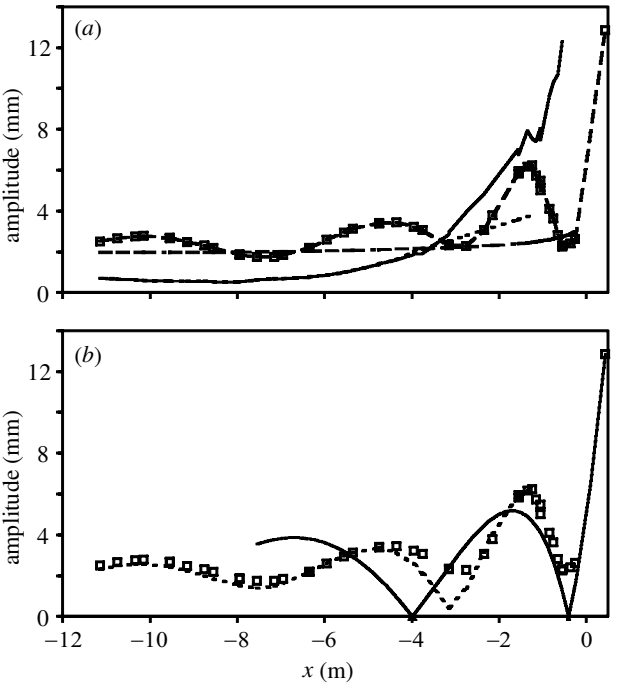

Figure 10. (*a*) Cross-shore variation in wave amplitude at $f_c = 0.207 \pm 0.018$ Hz, case J6033A. (▫ , data; solid line, IBLW; dashed line, IBLW (scaled); dot-dashed line, OFLW (inverse shoaling).) (*b*) Cross-shore variation in wave amplitude at $f_c = 0.207 \pm 0.018$ Hz compared with nodal structure of free-standing wave and the numerical solution, case J6033A. (▫ , data; solid line, J_0; dashed line, numerical solution.)

in accordance with the observations. Equation (4.4) is also consistent with field data obtained on a very mildly sloping beach, showing free long-wave amplitudes to be approximately proportional to the square root of the offshore wave height (Ruessink 1998).

(*e*) *Cross-shore structure of the long-wave motion*

This section examines the cross-shore structure of the long-wave motion in more detail and, in particular, the nodal structure formed by the interaction of the incident bound waves and the outgoing free long waves. Figure 10*a* shows the cross-shore variation in amplitude of the total long-wave motion, the outgoing free long wave (OFLW) and the incident bound long wave (IBLW) at $f_c = 0.207$ Hz for case J6033A. This frequency corresponds well with the peak outgoing long-wave energy (figure 4) and also exhibits the strongest cross-shore nodal structure (figure 9*d*). The incident bound wave amplitudes were calculated from the measured frequency spectra as outlined in § 3 *c*, again over the range f_2–f_1. Strong cross-shore gradients in the measured data occur close to the breakpoint, with an anti-node in the outer surf zone and a node close to the mean breakpoint position for this case ($x = -0.7$ m), in agreement with the Symonds *et al*. (1982) model. The nodal structure is weaker further offshore, consistent with the outgoing free wave dominating over the incident bound wave at this frequency.

Figure 10*b* shows the same data, together with an analytical solution for a free-standing long wave and a numerical solution describing the interaction of the incident bound long wave and outgoing free long wave. The standing-wave solution is simply given by a zero-order Bessel function (denoted by J_0), with a shoreline amplitude equal to that measured, origin at the mean cross-shore run-up position and valid for $x > -8$ m. The numerical solution was obtained by numerically integrating the phase functions for the two long waves along the length of the flume, each with the amplitudes shown in figure 10*a* (see Baldock *et al.* 2000 for further details). However, the bound long waves are formed through the interaction of multiple pairs of frequency components, and hence multiple wavenumber pairs (k_1, k_2), resulting in bound waves at the same frequency having different wavenumbers ($\Delta k = k_1 - k_2$). It is therefore necessary to determine a single representative wavenumber (K) for the bound wave energy at frequency f_c. This was obtained by averaging the wavenumbers (Δk) resulting from the interaction of all the dominant primary (linear) components of the frequency spectrum that give rise to bound waves in the frequency band $f_c \pm \delta f$. The calculations were restricted to the primary frequency band $0.5 < f < 0.8$ Hz to ensure that K was not biased by including very weakly energetic bound waves with higher wavenumbers. Nevertheless, over 80% of the primary short-wave energy lies within this frequency band, and therefore the calculations cover a frequency range that includes a large proportion of the total bound wave energy.

The remaining variable is the phase relationship in the outer surf zone between the outgoing free long wave and the incident bound wave. This is readily estimated from the work of Symonds *et al.* (1982) and Schäffer (1993), with a more detailed discussion given by Baldock *et al.* (2000). For example, at an instant in time when a short-wave amplitude maximum reaches the mean breakpoint, the contribution to the total long-wave surface elevation from the incident bound wave will be negative. At the same time, breakpoint-forced long waves will be radiated seaward and shoreward, with negative and positive amplitude, respectively. Half a group period later, when a wave group minimum reaches the breakpoint, both the incident bound wave elevation and the breakpoint-forced wave radiated directly seaward will be positive. In addition, for a nodal point at the mean breakpoint position (figures 9*d* and 10*a*), the breakpoint-forced wave radiated shoreward half a group period earlier will have reflected from the shoreline and returned, again with positive elevation, constructively interfering with the other long-wave components. Hence the incident bound wave and the total outgoing breakpoint-forced free wave will be in phase just seaward of the breakpoint, leading to the formation of the anti-node in the outer surf zone ($x \approx -1.2$ m, figure 10*a*). Conversely, if the incident bound long wave was released near the breakpoint and reflected from the shoreline, then the resulting seaward-propagating wave and incident bound long wave would be out of phase just seaward of the breakpoint.

Finally, it is well known that the solution of Longuet-Higgins & Stewart (1960, 1962) overestimates the amplitude of the bound waves in shallow water. Therefore, using a similar approach to that adopted by Baldock *et al.* (2000), we have scaled the amplitude of the bound wave, so that (accounting for phase) the sum of the incident bound wave and the outgoing long wave match the measured amplitude at the outer surf-zone anti-node. This typically requires a scaling factor of 0.6–0.3, consistent with the numerical results presented by Lo & Dean (1995), who showed that

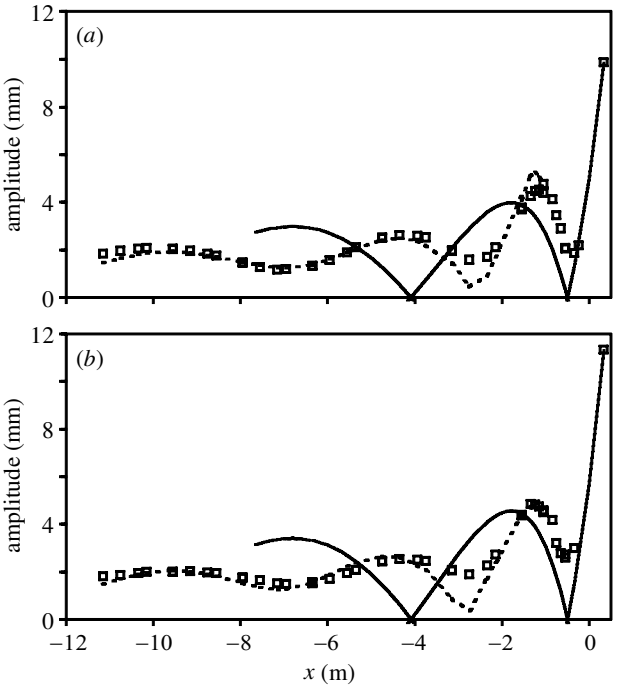

Figure 11. (*a*) Cross-shore variation in wave amplitude at $f_c = 0.207 \pm 0.018$ Hz compared with nodal structure of free-standing wave and the numerical solution, case J6033B. (□, data; solid line, J_0; dashed line, numerical solution.) (*b*) Cross-shore variation in wave amplitude at $f_c = 0.207 \pm 0.018$ Hz compared with nodal structure of free-standing wave and the numerical solution, case J6010B. (□, data; solid line, J_0; dashed line, numerical solution.)

Longuet-Higgins & Stewart's results overestimated the bound long-wave amplitude for $h/L_0 < 0.1$. This amplitude is then matched to that at $x = -4$ m ($h/L_0 > 0.1$), calculated as above from Longuet-Higgins & Stewart (1960), using a linear splice. This scaled solution is indicated by the dashed line in figure 10*a* and these amplitudes are subsequently used in the final numerical solution.

The data in figure 10*b* clearly suggest the generation of a (partial) standing wave in the inner surf zone, in agreement with both the breakpoint-forcing and bound wave release long-wave-generation models. However, further offshore, the standing-wave solution shows no correlation with the data. In addition, in the surf zone, the data also show that both the gradients in long-wave amplitude and the location of the anti-node differ from that expected for a linear free-standing long wave. Indeed, the shoreward shift in the position of the anti-node in the outer surf zone is consistent with the breakpoint forcing discussed above. Furthermore, close to and within the breaker zone, a released and reflected bound long wave should give rise to a nodal structure more in agreement with the linear standing-wave model, which is not borne out by the present results. In contrast, offshore of the breakpoint, the numerical solution provides an excellent description of the measured data, with both the amplitude and position of the nodal structure well described.

Similar data, and the corresponding standing wave and numerical solutions, are shown for two further cases, J6033B and J6010B, respectively, in parts (*a*) and (*b*) of

figure 11. In each case, a node occurs close to the mean breakpoint position, with an anti-node in the outer surf zone shifted shorewards compared with the standing-wave solution. The numerical solution, again with the incident bound wave and outgoing free long wave in phase at the anti-node position, also shows good agreement with the data. The mismatch between the measured data and the standing-wave solution again suggests that the outgoing long wave is not predominantly due to a released and reflected bound wave, unless a significant phase shift occurs during the propagation of the free long wave through the surf zone. However, no mechanism for such a phase shift has been proposed.

The data presented above strongly support the breakpoint-forcing model for long-wave generation proposed by Symonds *et al.* (1982) and extended by Schäffer (1993). In addition, the data show little evidence of incident bound long-wave release at the breakpoint and subsequent reflection. This is in contrast to much field data, typically from less-steep swell waves on mildly sloping beaches, which suggest that released and reflected bound waves may dominate over breakpoint-forced long waves (Tucker 1950; Guza *et al.* 1984; List 1992; Masselink 1995). However, in the present study, the dominant incident short waves in the frequency band $0.5 < f < 0.8$ only become shallow water waves ($h/L < \frac{1}{20}$) in the inner surf zone ($x > -0.5$ m). Therefore, the bound waves forced by interactions around the short-wave spectral peak also will not satisfy the shallow-water resonance condition ($\Delta k = 2\pi f/\sqrt{gh}$) for a free long wave until the inner surf zone. Consequently, since about half the incident short-wave energy is dissipated by breaking further offshore, the bound wave forcing in the inner surf zone will be much weaker than that outside the break point. Hence, if the bound wave is not released until the resonance condition is satisfied (List 1992), the resulting free long wave will be of small amplitude, in accordance with the present observations. It therefore appears that the long-wave forcing mechanism may be dependent on the characteristics of the incident waves, with breakpoint forcing possibly dominant during storm conditions, and bound long-wave release and reflection dominating with milder long-period swell waves. Further laboratory experiments simulating swell conditions would be beneficial to resolve this question.

5. Conclusions

New laboratory data have been presented on long-wave (surf-beat) forcing by shorter random gravity water waves. Eight different random wave series have been investigated, covering a range of short-wave amplitudes, peak spectral frequency and spectral shape. The data include incident and outgoing long-wave amplitudes, the correlation between forced long waves and random short-wave groups, the dependence of long-wave energy on short-wave energy, and a detailed analysis of the cross-shore structure of the long-wave motion. The observations are critically compared with two fundamentally different mechanisms for long-wave forcing (Longuet-Higgins & Stewart 1962, 1964; Symonds *et al.* 1982).

Seaward-propagating free long waves exhibit a strong frequency dependence, with the normalized long-wave amplitudes showing good quantitative and qualitative agreement with the breakpoint-forcing model proposed by Symonds *et al.* (1982). Maximum long-wave forcing occurs for $\chi \approx 1$–1.4, with minimal long-wave generation observed for χ in the range 3–4. In addition, the amplitudes of seaward-propagating

free long waves are found to be linearly dependent on the incident short-wave amplitude, in agreement with the theory and much field data. For constant incident wave groupiness, the surf beat also appears relatively insensitive to spectral shape.

Cross-correlations between the incident short-wave envelope and total low-frequency motion show incident bound waves negatively correlated with short-wave groups, with a lag close to zero, as expected from second-order wave theory (Longuet-Higgins & Stewart 1962). A second strong positive correlation at later lags is consistent with breakpoint-forced long waves propagating seaward, which contrasts with Tucker's (1950) data, but is in agreement with the observations of Munk (1949). A strong positive correlation between the run-up (swash) and incident wave groups offshore of the breakpoint is also inconsistent with the release of the incident bound long waves (Longuet-Higgins & Stewart 1962) as the primary surf-beat-generation mechanism in these experiments.

At the lowest long-wave frequencies ($f < 0.17$ Hz), the total long-wave energy seaward of the breakpoint is shown to be nonlinearly dependent on the incident short-wave energy and therefore dominated by incident bound long waves (Longuet-Higgins & Stewart 1962). However, in the same frequency range, the long-wave energy inside the surf zone and in the run-up appears much more linearly dependent on incident short-wave energy, suggesting that breakpoint-forced long waves dominate in this region. In contrast, close to the peak spectral frequency of the free long waves ($f \approx 0.24$ Hz), the long-wave energy is linearly dependent on the incident short-wave energy both offshore and inside of the breakpoint. The dominant long-wave motion for these random wave cases is therefore consistent with the long-wave forcing model proposed by Symonds *et al.* (1982).

A further detailed analysis of the cross-shore structure of the long-wave motion shows that maximum surf-beat generation occurs when the mean breakpoint position coincides with a nodal point for a free-standing long wave in the surf zone, again in agreement with the breakpoint-forcing model. Furthermore, a numerical solution describing the interaction of the incident bound long wave and outgoing free long wave shows that both these long-wave components are in phase just seaward of the mean breakpoint position. This is again consistent with long-wave forcing by the time-varying breakpoint, rather than by release and reflection of the incident bound waves. Finally, a probable reason for the absence of released and reflected bound long waves is that the shallow-water resonance condition is not satisfied until the incident short waves reach the inner surf zone. It is suggested that breakpoint-forced long waves may well dominate two-dimensional surf-beat motions during storm conditions, with released and reflected bound long waves dominating in conditions with milder long-period swell waves.

The authors gratefully acknowledge funding from the UK Engineering and Physical Sciences Research Council, grant no GR/R21974/01, and the European Commission through the MAST III programme, SASME project, contract no MAS3-CT97-0081. Thanks also to Ian Morgan, University of Plymouth, for producing figure 1.

References

Baldock, T. E., Swan, C. & Taylor, P. H. 1996 A laboratory study of non-linear surface waves on water. *Phil. Trans. R. Soc. Lond.* A **354**, 649–676.

Baldock, T. E., Huntley, D. A., Bird, P. A. D., O'Hare, T. J. & Bullock, G. N. 2000 Breakpoint generated surf beat induced by bichromatic wave groups. *Coastal Engng* **39**, 213–242.

Barthel, V., Mansard, E. P. D., Sand, S. E. & Vis, F. C. 1983 Group-bounded long waves in physical models. *Ocean Engng* **10**, 261–294.

Battjes, J. A. 1988 Surf zone dynamics. *A. Rev. Fluid Mech.* **20**, 257–293.

Bendat, J. S. & Piersol, A. G. 1986 *Random data, analysis and measurement procedures*. Wiley.

Bird, C. C. & Peregrine, D. H. 1998 Wave crest interaction in water of intermediate depth. In *Proc. 26th Int. Conf. Coastal Engineering*, pp. 98–111. New York: American Society of Civil Engineers.

Dally, W. R. & Dean, R. G. 1986 Transformation of random breaking waves on surf beat. In *Proc. 20th Int. Conf. Coastal Engineering*, pp. 109–123. New York: American Society of Civil Engineers.

Elgar, S. & Guza, R. T. 1985 Observations of bispectra of shoaling surface gravity waves. *J. Fluid Mech.* **161**, 425–448.

Elgar, S., Herbers, T. H. C., Okihiro, M., Oltman-Shay, J. & Guza, R. T. 1992 Observations of infragravity waves. *J. Geophys. Res.* **97**, 15 573–15 577.

Freilich, M. H. & Guza, R. T. 1984 Non-linear effects on shoaling surface gravity waves. *Phil. Trans. R. Soc. Lond.* A **311**, 1–41.

Frigaard, P. & Brorsen, M. 1995 A time domain method for separating incident and reflected irregular waves. *Coastal Engng* **24**, 205–215.

Gallagher, B. 1971 Generation of surf beat by non-linear wave interactions. *J. Fluid Mech.* **49**, 1–20.

Garrett, C. J. R. & Toulany, B. 1981 Variability of the flow through the Strait of Belle Isle. *J. Mar. Res.* **39**, 163–189.

Goda, Y. 1975 Irregular wave deformation in the surf zone. *Coastal Engng Jpn* **18**, 13–26.

Guza, R. T. & Thornton, E. B. 1982 Swash oscillations on a natural beach. *J. Geophys. Res.* **87**, 483–491.

Guza, R. T. & Thornton, E. B. 1985 Observations of surf beat. *J. Geophys. Res.* **90**, 3162–3172.

Guza, R. T., Thornton, E. B. & Holman, R. A. 1984 Swash on steep and shallow beaches. In *Proc. 19th Int. Conf. Coastal Engineering*, pp. 708–723. New York: American Society of Civil Engineers.

Hamm, L., Madsen, P. A. & Peregrine, D. H. 1993 Wave transformation in the nearshore: a review. *Coastal Engng* **21**, 5–39.

Hasselmann, K., Munk, W. H. & Macdonald, G. 1963 Bispectra of ocean waves. In *Time series analysis* (ed. M. Rosenblatt), pp. 125–139. Wiley.

Hasselmann, K. (and 15 others) 1973 *Measurements of wind-wave growth and swell decay during the Joint North Sea Wave Project (JONSWAP)*. Hamburg: Deutches Hydrographisches Institut.

Herbers, T. H. C., Elgar, S. & Guza, R. T. 1994 Infragravity-frequency (0.005–0.05 Hz) motions on the shelf I. Forced waves. *J. Phys. Oceanogr.* **24**, 917–927.

Herbers, T. H. C., Elgar, S., Guza, R. T. & O'Reilly, W. C. 1995 Infragravity-frequency (0.005–0.05 Hz) motions on the shelf II, Free waves. *J. Phys. Oceanogr.* **25**, 1063–1079.

Hibberd, S. & Peregrine, D. H. 1979 Surf and run-up on a beach: a uniform bore. *J. Fluid Mech.* **95**, 323–345.

Holman, R. A. & Bowen, A. J. 1982 Bar, bumps and holes: models for the generation of complex beach topography. *J. Geophys. Res.* **87**, 457–468.

Huang, N. E., Shen, Z. & Long, S. R. 1999 A new view of nonlinear water waves: the Hilbert spectrum. *A. Rev. Fluid Mech.* **31**, 417–457.

Huntley, D. A., Guza, R. T. & Bowen, A. J. 1977 A universal form for shoreline run-up spectra? *J. Geophys. Res.* **82**, 2577–2581.

Huntley, D. A., Guza, R. T. & Thornton, E. B. 1981 Field observations of surf beat 1. Progressive edge waves. *J. Geophys. Res.* **86**, 6451–6466.

Janssen, T. T., Kamphuis, J. W., Van Dongeren, A. R. & Battjes, J. A. 2000 Observations of long waves on a uniform slope. In *Proc. 27th Int. Conf. Coastal Engineering*, pp. 2192–2205. New York: American Society of Civil Engineers.

Jenkins, G. M. & Watts, D. G. 1968 *Spectral analysis and its applications*. San Francisco, CA: Holden-Day.

Kobayashi, N., DeSilva, G. S. & Watson, K. D. 1989 Wave transformation and swash oscillation on gentle and steep slopes. *J. Geophys. Res.* **94**, 951–966.

Kostense, J. K. 1984 Measurement of surf beat and set-down beneath wave groups. In *Proc. 19th Int. Conf. Coastal Engineering*, pp. 724–740. New York: American Society of Civil Engineers.

List, J. H. 1991 Wave groupiness in the nearshore. *Coastal Engng* **15**, 479–496.

List, J. H. 1992 A model for the generation of two-dimensional surf beat. *J. Geophys. Res.* **97**, 5623–5635.

Lo, J. M. & Dean, R. G. 1995 Long waves due to interactions beneath wave groups. *J. Wtrwy Port Coastal Ocean Engng* **121**, 317–325.

Longuet-Higgins, M. S. & Stewart, R. W. 1960 Changes in the form of short gravity waves on long waves and tidal currents. *J. Fluid Mech.* **8**, 565–583.

Longuet-Higgins, M. S. & Stewart, R. W. 1962 Radiation stress and mass transport in gravity waves, with application to 'surf beats'. *J. Fluid Mech.* **13**, 481–504.

Longuet-Higgins, M. S. & Stewart, R. W. 1964 Radiation stress in water waves: a physical discussion with applications. *Deep Sea Res. I* **11**, 529–562.

Madsen, P. A., Sorensen, O. R. & Schaffer. H. A. 1997 Surf zone dynamics simulated by a Boussinesq type model. Part 2. Surf beat and swash oscillations for wave groups and irregular waves. *Coastal Engng* **32**, 289–319.

Masselink, G. 1995 Group bounded long waves as a source of infragravity energy in the surf zone. *Continent. Shelf Res.* **15**, 1525–1547.

Mei, C. C. & Benmoussa, C. 1984 Long waves induced by short wave groups over an uneven bottom. *J. Fluid Mech.* **139**, 219–235.

Munk, W. H. 1949 Surf beats. *Trans. Am. Geophys. Union* **30**, 849–854.

O'Hare, T. J. & Huntley, D. A. 1994 Bar formation due to wave groups and associated long waves. *Mar. Geol.* **116**, 313–325.

O'Hare, T. J., Baldock, T. E., Huntley, D. A., Bird, P. A. D. & Bullock, G. N. 2000 Free long wave–short wave interaction in a surf zone. In *Proc. 27th Int. Conf. Coastal Engineering*, pp. 1448–1461. New York: American Society of Civil Engineers.

Oltman-Shay, J. & Guza, R. T. 1987 Infragravity edge wave observations on two California beaches. *J. Phys. Oceanogr.* **17**, 644–663.

Osborne, P. D. & Greenwood, B. G. 1992 Frequency dependent cross-shore suspended sediment transport 1. A non-barred shoreface. *Mar. Geol.* **106**, 1–24.

Peregrine, D. H. 1983 Breaking waves on beaches. *A. Rev. Fluid Mech.* **15**, 149–178.

Roelvink, J. A. 1993 Surf beat and its effect on cross-shore profiles. PhD. thesis, Technical University of Delft.

Ruessink, B. G. 1998 Bound and free infragravity waves in the nearshore zone under breaking and nonbreaking conditions. *J. Geophys. Res.* **103**, 12 795–12 805.

Schäffer, H. A. 1993 Infragravity waves induced by short wave groups. *J. Fluid Mech.* **247**, 551–588.

Sobey, R. J. & Liang, H.-B. 1986 Complex envelope identification of wave groups. In *Proc. 20th Int. Conf. Coastal Engineering*, pp. 752–766. New York: American Society of Civil Engineers.

Suhayda, J. N. 1974 Standing waves on beaches. *J. Geophys. Res.* **79**, 3065–3071.

Symonds, G., Huntley, D. A. & Bowen, A. J. 1982 Two-dimensional surf beat: long wave generation by a time-varying breakpoint. *J. Geophys. Res.* **87**, 492–498.

Tucker, M. J. 1950 Surf beats: sea waves of 1 to 5 min period. *Proc. R. Soc. Lond.* A **202**, 565–573.

Van Dongeren, A. R., Sancho, F. E., Svendsen, I. A. & Putrevu, U. 1994 SHORECIRC: a quasi-3D nearshore model. In *Proc. 24th Int. Conf. Coastal Engineering*, pp. 1321–1334. New York: American Society of Civil Engineers.

Van Leeuwen, P. J. & Battjes, J. A. 1990 A model for surf beat. In *Proc. 22nd Int. Conf. Coastal Engineering*, pp. 32–40. New York: American Society of Civil Engineers.

Watson, G. & Peregrine, D. H. 1992 Low frequency waves in the surf zone. In *Proc. 23rd Int. Conf. Coastal Engineering*, pp. 818–831. New York: American Society of Civil Engineers.

Watson, G., Barnes, T. C. D. & Peregrine, D. H. 1994 The generation of low frequency waves by a single wave group incident on a beach. In *Proc. 24th Int. Conf. Coastal Engineering*, pp. 776–790. New York: American Society of Civil Engineers.

Wright, L. D., Guza, R. T. & Short, A. D. 1982 Dynamics of a high energy dissipative surf zone. *Mar. Geol.* **45**, 41–62.

Yu, J. & Mei, C. C. 2000 Formation of sand bars under surface waves. *J. Fluid Mech.* **416**, 315–348.